Cold-active alkaline phosphatase is irreversibly transformed into an inactive dimer by low urea concentrations.

Jens Guðmundur Hjörleifsson[1]* and Bjarni Ásgeirsson[1]*

[1]Department of Biochemistry, Science Institute, University of Iceland, Dunhagi 3, 107 Reykjavik, Iceland.

* Corresponding authors: Bjarni Ásgeirsson, email: bjarni@hi.is and Jens Guðmundur Hjörleifsson, email: jgh4@hi.is

Abstract:
Alkaline phosphatase, is a homodimeric metallo-hydrolase, where both Zn^{2+} and Mg^{2+} are important for catalysis and stability. Cold-adapted alkaline phosphatase variants have high activity at low temperatures and lower thermal stability compared with variants from mesophilic hosts. The instability, and thus inactivation, could be due to loose association of the dimers and/or loosely bound Mg^{2+} in the active site, but this has not been studied in detail for the cold-adapted variants. Here, we focus on using the intrinsic fluorescence of Trp in alkaline phosphatase from the marine bacterium *Vibrio splendidus* (VAP) to probe for dimerization without chemical modifications. Trp $\rightarrow$ Phe substitutions showed that two out of the five native Trp residues contributed mostly to the fluorescence emission. One residue, 15 Å away from the active site (W460) and highly solvent excluded, was phosphorescent and had a distant role in substrate binding. An additional Trp residue was introduced to the dimer interface to act as a possible probe for dimerization. Urea denaturation curves indicated that an inactive dimer intermediate, structurally equivalent to the native state, was formed before dimer dissociation took place. This is the first example of the transition of a native dimer to an inactive dimer intermediate for alkaline phosphatase without using mutagenesis, ligands, or competitive inhibition.

Keywords: Alkaline phosphatase, dimer, enzyme kinetics, protein fluorescence, phosphorescence, cold adaption.

1. Introduction

Alkaline phosphatase (AP) is one of the most extensively studied enzymes and yet its role is still not fully understood [1-3]. It catalyzes the hydrolysis of phosphomonoesters and is generally believed to be only active as a homodimer. The active site in each monomer consists of three conserved metal ion sites. The M1 and M2 sites are occupied by Zn^{2+} whereas the M3 site is generally occupied by Mg^{2+} and in some cases exchanged by Co^{2+} [4-6].

The role of the metal ions in catalysis and substrate binding has been extensively studied in *E. coli* AP [7-10] and mammalian APs [11, 12]. For *E. coli* AP (ECAP), the generally proposed reaction mechanism has the Zn^{2+} ions in M1 and M2 coordinating the binding of the monophosphate substrate, as well as activating the Ser102 nucleophile [13].

The role of Mg^{2+} is not fully clear. In crystallographic structures, the Mg2+ is usually octahedrally bound where a water molecule is coordinated between the Ser102 and Mg^{2+} [8, 13, 14]. The Mg2+ has been postulated to act as a general base, activating the nucleophilic Ser102. Earlier reports have also suggested a stabilizing role of Mg2+ for ECAP against inactivation during storage [15, 16]. Clearly, the role of Mg^{2+} is different for many alkaline phosphatases, where the Mg^{2+} can have activating role [17] as well as stabilizing role, or simply no effect [18]. Lastly, Mg^{2+} may be the deciding factor in bringing about discrimination between phosphoryl-hydrolysis from different substrates, e.q. monoesters and diesters [19].

The alkaline phosphatase studied here (VAP) was originally isolated from *Vibrio splendidus* [20], a gram negative and cold-adapted marine bacterium closely related to *E. coli.* It has one of the highest reported catalytic activity for APs, being adapted to work at cold temperatures [20, 21]. Furthermore, it has the lowest reported thermal stability of known APs with half-life less than 10 minutes at 40°C [20, 22] as well as the activity being very sensitive to urea [22, 23]. By replacing active-site residues involved in Mg^{2+} coordination with corresponding residues in the mesophilic ECAP namely D153 and K328, thermo-stability as well as resistance to urea increased [22]. Thus, it has been postulated that VAP binds magnesium weaker than other APs, hence the thermo-instability when activity is being monitored. Another possibility is that the active dimers in VAP are very weakly associated, leading to enzyme inactivation via dimer dissociation (VAP has inactive monomers). Recently, we made the enzyme variant R336L, where at least two hydrogen bonds at the interface should be broken. This mutant showed extreme thermo-instability and its activity dropped by half at 0.1 M of urea within half an hour (unpublished results). Thus, at present, it has not been established if VAP instability is governed by a weakly bound Mg^{2+} at the M3 site or by an instable dimer. Another possibility is that dimer association is cooperatively linked to Mg^{2+} binding.

To better understand the inactivation and unfolding pathway of VAP, a method to study the dimer dissociation event is needed. Many methods have been applied to study dimerization of various APs where the most common methods are size-exclusion chromatography (SEC) [24] and sedimentation velocity [25, 26]. Our group previously used SEC to study dimer dissociation in AP from Atlantic cod where the dimer dissociation was shown to be linked to loss of activity in the 2-3 M urea range [27]. SEC however has several drawbacks to study homodimer/monomer equilibrium. 1) In many cases SEC data has poor resolution leading to biased assignment of peaks, making data usually only qualitatively reliable, 2) resin interaction with proteins is known to occur, and 3) local concentration and solubility on SEC columns during runs can affect the dimer/monomer dissociation equilibrium. Shrimp AP was initially believed to be active as a monomer judged by SEC data as well as by native PAGE activity staining [28], but was later found to crystallize as a dimer [8]. The same conclusion was initially drawn for VAP for the same reasons [20], before the crystal structure was obtained [21].

Fluorescence of proteins is the most preferable real-time method to study quaternary structure dissociation due to its sensitivity and ability to work at physiological conditions. In addition to fluorescence, phosphorescence has been utilized to study metal ion binding [7] and phosphate binding [29] in ECAP. Only deeply buried Trp residues, like Trp109 in ECAP, have the propensities to have an electron transition to the long-lived triplet state. The absence of quenching residues nearby, or protein backbone interference, is a crucial factor as well [30]. Chemical incorporation of fluorescence probes can also be used to study homodimer dissociation, such as by fluorescence resonance energy transfer (FRET), however using extrinsic probes can affect either activity and/or stability of subunit association.

In order to report on the folded state of proteins, Tyr or Trp need to be in a position in the native fold so that upon dissociation a change in fluorescence signal is detected, e.g. residues are relieved of quenching by a nearby group, or a change in local polarity around the fluorophore is observed (spectral shifts). VAP has five Trp residues where no residue is located at the dimer interface. Thus, upon dissociation of dimers, the change in fluorescence signal due to monomer dissociation is insignificant, since it has been shown in the case of ECAP that the structure change of monomers upon dissociation is minimal [31].

In this study, all of the tryptophan residues of VAP were characterized with respect to fluorescence by making tryptophan to phenylalanine substitutions. An additional tryptophan residue was also introduced at the dimer interface. Urea induced fluorescence redshift and size exclusion chromatography were used to study the mechanism of inactivation and unfolding, in addition to the assessment of activity and global stability of the variants.

2. Materials and methods

2.1 Materials.

Chemicals were generally obtained from Sigma-Aldrich (Schnelldorf, Germany) or Merck (Darmstadt, Germany). Strep-Tactin Sepharose, (2-(4'-hydroxy-benzene-azo) benzoic acid (HABA), desthiobiotin and anhydrotetracyclin (AHTC) were from IBA GmbH (Germany). Bacto Yeast extract was obtained from Becton, Dickinson and Company (France). Primers were obtained from TAG (Copenhagen). Pfu polymerase, DnpI nuclease and markers were from Fermentas (St. Leon-Rot, Germany). Alkaline phosphatase from *E. coli* and other proteins were purchased from Sigma-Aldrich.

2.2 Generation of enzyme variants.

VAP was sub-cloned from an original pBluescript vector to a pASK3-plus StrepTactin vector (IBA, Gottingen, Germany). BsaI site overhangs were introduced in a PCR reaction using the forward oligonucleotide primer: 5'TAATGA**GGTCTCna**ATGAAACCAATTGT TACCGCA-3 and reverse primer: 5'-CAAAAA**GGTCTCngcgc**GTTTACTTG TTGTTTAATGT, where the BsaI binding site is shown in bold (cleavage sites in bold/lower letters) and the gene complimentary region is underlined. The PCR product was ligated into pASK3-plus digested with BsaI, giving a two amino acid linker between the gene C-terminus and the C-terminally linked StrepTag (WSHPQFEK).

Site-directed mutagenesis was performed using the QuikChange® kit (Stratagene) following the manufacturer´s protocol. Oligonucleotide primers were synthesized by TAG (Copenhagen, Denmark). All plasmids were propagated in *E. coli* TOP10 cells and plasmids were purified using NucleoSpin® plasmid purification kit (Macherey-Nagel, Germany) following the manufacturers protocol, or by co-precipitation with glycogen (Fermentas R0561 molecular biology grade) in ethanol following the manufacturer's protocol. Generally, three clones were sent for sequencing (Beckman Genomics, United Kingdom) and a positive clone selected and further expressed in the *E. coli* LMG194 strain (lacking an AP gene).

2.3 Protein expression and purification.

A single colony of LMG194 cells, previously transformed with mutated plasmid, was added to a 20 ml LB medium containing 0.1 mg/mL ampicillin (LAMP medium) and incubated at 37°C until a saturated culture was obtained (no more than 16 h). Approximately 2 ml of this starter culture were added to 450 mL of freshly prepared sterilized LAMP medium in total of nine bottles (4 L). Cells were grown at 18°C on an orbital shaker at 150 rpm until OD600 was 0.5-0.7. Then, anhydrotetracyclin was added to a final concentration of 20 ng/mL to induce expression. Cells were harvested 24 h later by centrifugation. The cell pellet was re-

suspended in lysis buffer (25 mM Tris, 10 mM $MgCl_2$, 0.5 mg/mL hen egg lysozyme, 0.01% Triton X-100, pH 8.0) and incubated at 2-4 h at 4°C before being frozen at -20°C. The cell lysate was allowed to slowly thaw and DNAse added to a final concentration of 0.050-0.10 mg/ml. The lysate was further incubated for 1-2 h at 4°C and finally centrifuged at 15.000 xg for 15 min to obtain a clear lysate.

For all variants except the W512F, where the tryptophan is located within the StrepTag sequence, the clear lysate was loaded onto a Strep-Tactin® affinity column (previously equilibrated in binding buffer: 25 mM Tris, 10 mM $MgCl_2$, pH 8.0) overnight at 4°C with a flow-rate of less than 0.1 ml/min. Nonspecifically bound proteins were washed off with 25 mM Tris, 10 mM $MgCl_2$, 150 mM NaCl, pH 8.0. The column was then equilibrated with binding buffer before eluting with elution buffer (25 mM Tris, 10 mM $MgCl_2$, 15% (v/v) ethylene glycol, 2.5 mM desthiobiotin, pH 8.0). Typical protein yield was between 3-5 mg of pure enzyme.

The W512F variant with a non-functional StrepTag was purified directly on L-histidyldiazobenzylphosphonic acid agarose column specific for alkaline phosphatases (Sigma-Aldrich) using the same conditions as for Strep-Tactin purification, except elution was done in 100 mM Na_2HPO_4, pH 9.1. Active fractions were pooled and dialyzed overnight in 2.0 L of 25 mM Tris, 10 mM $MgCl_2$, pH 8.0.

The W301F variant required further purification after Strep-Tactin column elution. The eluted enzyme from the Strep-Tactin purification was loaded onto a Mono-Q ion-exchange column and eluted using a 0-1 M NaCl gradient on a FPLC apparatus (GE-Healthcare).

Purity was analyzed by SDS-PAGE on 4-12% bis-Tris NUPAGE® (Invitrogen) gels. All purified enzyme samples contained 15% (v/v) ethylene glycol and were snap-frozen in liquid nitrogen before storing at -20°C.

2.4 Fluorescence measurements

All enzyme variants were diluted from approximately 0.4-0.5 mg/ml stock solutions to 0.02 mg/mL in buffer containing 20 mM Mops, 1 mM $MgSO_4$, pH 8.0 (10°C). Emission spectra were recorded at 10°C on a FluoroMax4 (Horiba) with 0.5 nm increments and consisted of three averaged scans. An excitation wavelength of 295 nm was selected and a slit-width of 5.0 nm was used for both excitation and emission. The relatively high excitation slit-width of 5 nm did not cause significant photo-bleaching during measurements. A blank solution spectrum was measured under the same conditions and subtracted from the other spectra. The wavelength of maximum emission intensity (λ_{max}) was determined by fitting the spectra to a 3rd degree polynomial in the range 315-370 nm ($y = ax^3 + bx^2 + cx + d$, where y is intensity and x is wavelength. The roots of the first derivative were solved by solving the quadratic equation for the polynomial.

Acrylamide was chosen for collisional quenching studies for three reasons: Acrylamide quenching efficiency (f_Q) of tryptophan is near unity [32], acrylamide is uncharged, so charge effects are absent, and acrylamide is capable of long-range interactions with tryptophan in proteins, so quenching can be observed without direct penetration [33, 34]. Collisional quenching of fluorescence is described by the Stern-Volmer equation:

$$F_0/F = 1 + k_q \tau_0[Q] = 1+ K_{sv}$$

Where F_0 and F are the fluorescence intensities in the absence and presence of quencher, respectively, k_q is the bimolecular quenching constant, t_0 is the lifetime of fluorescence without quencher, Q is the concentration of quencher and K_{sv} is the Stern-Volmer constant for collisional quenching.

Fluorescence measurement for acrylamide quenching was done as described above after adding aliquots from a 5.0 M stock solution of acrylamide giving concentrations in the range 0 - 0.3 M acrylamide (sample dilution by each added aliquot was corrected for). By plotting F_0/F against [acrylamide], the slope of the linear fit is the Stern-Volmer constant, K_{sv}.

2.5 Urea denaturation and inactivation measurements.

Samples were incubated for 4 h at 10 °C with varying concentration of urea ranging from 0-8 M in 25 mM Mops, 1 mM $MgSO_4$, pH 8.0. Tryptophan fluorescence was monitored as described above, where wavelength of maximum emission intensity (λ_{max}) was determined. For enzyme inactivation experiments, samples were incubated in urea in the range of 0-2 M. Activity was measured under transphosphorylating conditions using 2.0 mM p-nitrophenyl phosphate (p-NPP) in 1.0 M diethanolamine with 1.0 mM $MgCl_2$ at pH 9.8 and 10 °C. The change in absorbance was followed at 405 nm over a 30 sec period in a temperature regulated Evolution 220 spectrophotometer (Thermo Scientific). An extinction coefficient of 18.5 $M^{-1}cm^{-1}$ was used at pH 9.8. The unfolding curves were fitted to a two state model for the wild-type VAP ($N \rightarrow D$) and a three state model for the F355W variant ($I_2 \rightarrow 2I \rightarrow 2D$) using the open-source graphical freeware CDpal [35].

2.6 Phosphorescence measurements.

Phosphorescence of samples was measured in 20 mM Tris, 10 mM $MgCl_2$, pH 8.0 at 10 °C on a Horiba Fluormax4-P using a xenon pulsed lamp equipped with a R928P photon-counting detector. Samples were degassed by argon-purging in a closed flow-cell cuvette for 1 h on ice before performing measurements. Concentration was 5-6 µM for VAP and ECAP, and 8 µM for W460F. Phosphorescence spectra were measured using excitation at 292 nm with 5 nm

slit width for both excitation and emission. A gate-and-delay generator was used to measure phosphorescence decay by increasing the initial delay from 1 ms to 180 ms in 2 ms intervals using 290 nm and 440 nm for excitation and emission, respectively. The excitation and emission slit-widths were 5 nm and 10 nm, respectively. Each interval consisted of 50 measured pulses with a sample window of 200 ms. The data were initially fitted to a single-exponential curve $I(t) = \alpha \cdot e^{-t/\tau}$,where I is intensity, α is the pre-exponential factor, t is time and τ is the lifetime. While this analysis was sufficient for ECAP, wild-type VAP and the VAP-W460F variant required a double-exponential fit, $I(t) = \alpha_1 \cdot e^{-t/\tau 1} + \alpha_2 \cdot e^{-t/\tau 2}$.

2.7 Enzyme kinetics.

Enzyme kinetic rate constants were determined at 10°C by measuring the turnover-rate under hydrolyzing conditions using varying concentrations of p-nitrophenyl phosphate (p-NPP) in 0.1 M CAPS, 1 mM $MgCl_2$, 0.5 M NaCl, pH 9.8 (corrected for 10°C) over 30 sec period in a temperature regulated Evolution 220 spectrophotometer (Thermo Scientific). For exact determination of initial pNPP concentration for each measurement, the sample was allowed to fully hydrolyze and concentration determined by measuring the absorbance at 405 nm (using extinction coefficient 18.5 $mM^{-1}cm^{-1}$). Enzyme concentration was measured by absorption at 280 nm using extinction coefficient of 61310 $M^{-1}cm^{-1}$, 55935 $M^{-1}cm^{-1}$ and 66810 $M^{-1}cm^{-1}$ for wild-type, Trp → Phe variants and Phe → Trp variants respectively [36].

K_M and k_{cat} were determined by non-linear regression fit to the Michaelis–Menten equation using GraphPad Prism®.

2.8 Thermal unfolding measurements.

Enzyme samples with absorbance at 280 nm between 0.1-0.2 were dialyzed overnight in 25 mM Mops, 1 mM $MgSO_4$ at pH 8.0 (20 °C). T_m determination was performed on a JASCO J-810 circular dichroism (CD) spectropolarimeter by measuring a melting curve at 222 nm in the range 15-85 °C in a 2 mm cuvette with 1°C/min temperature rise. A two-state pathway was assumed for monomer unfolding N ⇆ U, where N is native and U unfolded enzyme. The traces were normalized and T_m determined at F_U by a direct fit to a sigmoidal curve using the program Kaleidagraph®.

2.9 Size exclusion chromatography

Chromatography was performed on a Pharmacia FPLC apparatus equipped with a Superose 12 column (GE Healthcare). The column was pre-equilibrated at 0.5 ml/min and temperature of 4-5 °C with three column volumes of the same denaturant solution as used for pre-incubating the samples. The buffer was 25 mM Mops, 1 mM $MgSO_4$ (pH 8.0) containing urea

where indicated. The final enzyme concentration was ≈ 1.5 mg/ml (25 μM) and the samples were applied in a volume of 0.5 ml. The column was calibrated with the following standard proteins: immunoglobulin G (150 kDa), egg albumin (45 kDa), pepsin (35 kDa), myoglobin (16 kDa), and cytochrome c (11.6 kDa).

3. Results

3.1 Trp substitutions in VAP.

Vibrio alkaline phosphatase (VAP) has five native Trp residues and one extra Trp located on the StrepTag® purification tag which is likely fully exposed and mobile. The StrepTag variant of the wild-type VAP gave an identical x-ray structure to the one previously published without a C-terminal tag (Figure 1A) and no diffractions were observed from the tag (Helland & Asgeirsson, unpublished results). All of the Trp residues in VAP are highly conserved in known bacterial APs, except W475 and W155 (Figure 1B). None of the Trp residues are located on the four designated non-homologous inserts previously reported in VAP [21]. W155, W301 and W475 are all located in the typical αβα-folded center and are buried, or partially buried, between the strands and helices in the fold (Figure 1 C-H). The environment is highly non polar for W155, while for W301, W460 and W475 the environment has a distinctive amphipathic character with one side around the tryptophan residue non-polar and the other polar. The W460 residue is located on a short loop at a conserved site buried below the roots of the so-called crown domain, 15 Å away from the active site and 5 Å away from the backbone of the other monomer. Even so, W460 is not counted here as an interface residue in the usual sense, since the residue points inwards toward the tertiary core. W274 is located in the active site and nearly fully exposed. It binds a water molecule that is additionally hydrogen bonded to another water molecule bound to the active-site Mg^{2+}.

FIGURE 1 here.

Single Trp substitutions to phenylalanine were made to study the role of each Trp in VAP emission spectrum. All variants were expressed as soluble enzymes with yields comparable to wild-type expression yield, except for W301F, where the yield for soluble enzyme was 10-20 times lower, and the enzyme was possibly precipitated as inclusion bodies to some extent. W301F required further purification after affinity purification to remove two extra bands seen in SDS-PAGE that were consistently present as co-eluents.

A new Trp residue was introduced by forming the F355W variant as a strategy to introduce a Trp residue at the dimer interface to serve as a probe for dimerization. F355 is located at the

root of the long surface loop that characterizes this particular AP in comparison with ECAP (Figure 1B and H). This site was chosen for further studies, since we found that a mutation to a Tyr at this site had no effect on kinetics or thermal stability, indicating structural neutrality at this site.

3.2 Kinetic constants and stability of the Trp→ Phe variants

Enzyme kinetics were performed under hydrolyzing conditions. Recently, we have added 500 mM NaCl to our kinetic sample buffer since it has a stabilizing effect for storage, both on ice and at room temperature. Figure 2A shows the high stabilizing effect 500 mM NaCl has on VAP at room temperature, where activity does not drop for two days. After 4 days with NaCl present the activity was still 75% of initial activity. Without NaCl the activity dropped steadily and after 1 day 10 % of activity remained. Furthermore, NaCl increased the enzymes catalytic turnover where the activity peaked at a salt concentration of 500 mM (Figure 2B). Concurrently, K_M was increased approximately twofold at 500 mM NaCl (data not shown). This activity enhancement is believed to come from the chloride anion since the same effect is seen using KCl.

TABLE 1 here and Figure 2

The W512F variant (tryptophan located on the C-terminal StrepTag) showed no significant change for either k_{cat} or K_M compared with the wild-type VAP that showed a k_{cat} and K_M of 302 ± 20 s^{-1} and 194 ± 30 μM, respectively. The W274F mutant, where an exposed Trp was removed from the active site, maintained the same activity as the wild-type. The k_{cat} decreased for all the other variants, being 125 ± 2 s^{-1}, 137 ± 8 s^{-1}, 65 ± 4 s^{-1} and 44 ± 2 s^{-1} for W155F, W301F, W460F and W475F, respectively. The K_M values remained unchanged compared with wild-type, except for W460F and W274F, where the K_M was 1.8-fold and 2.5-fold higher than the wild-type value, respectively. Overall, W460F had the lowest catalytic efficiency (k_{cat}/K_M) of 184 $s^{-1}mM^{-1}$ compared to 1460 $s^{-1}mM^{-1}$ for the wild-type.

In order to understand better the role of W460 in catalysis, the W460Y (Tyr or Trp is conserved at this position) and W460I (non-polar branched residue) variants were made. The W460Y variant showed only minimal decrease in k_{cat} (275 ± 4 s^{-1}) and a slight increase in K_M (252 ± 46 μM) compared to the wild-type, while the W460I variant was completely inactive.

Melting temperatures (T_m) were determined by CD spectroscopy as an indication of monomer unfolding (Table 1 and Figure S1-A). Magnesium and the competitive inhibitor-ion sulphate affected the stability of the monomers (Figure S1-B), so we used a moderate concentration of 1 mM $MgSO_4$ in the sample buffer for melting temperature experiments. No change in T_m was observed for the W512F (51.0 ± 0.6 °C) variant compared to wild-type (51.0 ± 0.3 °C). For all the other variants, a decrease in T_m was seen at 49.8 ± 2.2 °C, 47.1 ±

0.7 °C, 44.6 ± 1.7 °C, 48,7 ± 1.3 °C and 48.1 ± 0.1 for W155F, W274F, W301F, W460F and W475F, respectively. The large decrease in T_m observed for the W301F variant indicated a loosening of the globular fold.

3.3 Trp → Phe variant emission spectra and acrylamide quenching

Tryptophan emission spectra for all the enzyme variants are shown in Figure 3A. The W512F change located on the StrepTag had no effect on the emission spectra, indicating that W512 is completely solvent exposed and likely quenched by a nearby group, possibly the histidine residue in the tag (residue number 3). It is clear, that the dominant fluorescence signal comes from W460 and W301, as variants W460F and W301F showed a close to 50% decrease in fluorescence intensity individually compared to the wild-type VAP. The W274F variant showed increased fluorescence compared to the wild-type VAP. This can be explained by a change in conformation around one or more remaining Trp, where static quenching by nearby residue has been relieved. The W155F variant had a slightly lower emission signal than the wild-type, while W475F showed a moderate decrease.

FIGURE 3 here.

From the data in Figure 3A it is also apparent, that one or more of the Trp → Phe alterations affected the packing and/or structure of the enzyme, since the sum of the difference spectra for the Trp → Phe variants compared to wild-type VAP emission was higher than the emission of wild-type VAP. This was most noticeable at the blue edge of the emission spectra (W274F was excluded since the difference there < 0).

To examine solvent exposure of Trp-residues in VAP, the wavelength of maximum emission (λ_{max}) was determined (Table 2). Overall, the Trp-substitutions had only a moderate effect on λ_{max}. For the wild-type VAP, the λ_{max} was 340.1 ± 0.1 nm while the exposed Trp residue mutants, W274F and W512F, showed a modest blue-shift to λ_{max} 339.3 ± 0.2 nm and 339.5 ± 0.3 nm, respectively. This correlates with removal of a Trp residue that is more exposed than the average of the set of tryptophans. Removal of the residues that showed decreased emission upon removal, W155F, W301F, W460F and W475F, resulted in a moderate red-shift in all cases with λ_{max} of 341.1 ± 0.1 nm, 341.0 ± 0.1 nm, 341,4 ± 0.8 nm and 342.0 ± 0.1 nm, respectively. This correlates with the removal of a residue more buried than the average.

TABLE 2 here.

To further examine solvent exposure of the Trp residues, acrylamide collisional studies were conducted. Measurements were plotted as Stern-Volmer plots (Figure 3B) and the calculated Stern-Volmer constants, K_{sv} are shown in Table 2. In the concentration range of 0 - 0.3 M acrylamide, all the variants showed no deviation from linearity in the Stern-Volmer plots. All variants had similar Stern-Volmer constants as wild-type VAP (2.4 ± 0.3 M^{-1}), except W460F, which showed a striking 3.3 fold increase in the Stern-Volmer constant (7.9 ± 0.2 M^{-1}). This indicated that upon W460 removal, the remaining residues became more prominent in their contribution to the signal. In other words, W460 is likely almost completely shielded from the solvent. Not even acrylamide, which is known to have long range quenching effect deep into protein cores [36], is able to reach W460 and quench its emission.

3.4 Room-temperature phosphorescence measurements

Only Trp residues buried deeply away from the solvent in protein-cores are capable of having long emission lifetimes in aqueous buffer solutions at room temperature. Such excited state is the result of interstate crossing from the singlet state to the long-lived triplet state. It is also well known, that oxygen is a very efficient collisional quencher of phosphorescence. Thus, samples need to be deoxygenated efficiently before measuring can proceed. Furthermore, phosphorescence is often quenched statically by a nearby intrinsic quencher, mainly His, Tyr, Trp and Cys residues [30]. None of these residues are within 5 Å proximity of W460, which is a likely candidate to be phosphorescent at room temperature in VAP.

FIGURE 4 here.

Indeed, VAP was found to be phosphorescent at 20 °C, having a typical red-shifted phosphorescence emission spectrum (Figure 4A) with two maxima at 418 nm and 443 nm, similar in shape as the ECAP phosphorescence spectrum at room temperature [7, 29]. Phosphorescence decay curves are shown in Figure 3B where VAP wild-type phosphorescence decay fitted best to a double exponential decay with one long lifetime of 140 ms and one short lifetime of 40 ms. The latter had a 17% relative amplitude. To define whether the two lifetimes originated from the same Trp molecule, phosphorescence decay of W460F was recorded. W460F also showed phosphorescence, although the signal was roughly 10 times less intense than for the wild-type VAP and correlated well with the low relative amplitude of the shorter 40 ms lifetime. The W460F decay curve was fitted to a double exponential decay equation, where the lifetimes were 6 ms and 65 ms, The shorter lifetime of W460F might arise from background during acquisition due to higher signal to noise ratio, or

a third phosphorescent tryptophan with very a low phosphorescence yield not detectable when W460 is present.

As a control, ECAP phosphorescence was also recorded. In our hands, the ECAP phosphorescence decay was fitted to a single exponential decay function and had a lifetime of 230 ms which is considerably shorter than published values [37]. Thus, it was clear that our oxygen purging system, by slowly blowing argon gas through a quartz flow-cell, was not working to fully remove all oxygen from the sample. We calculated that the oxygen concentration after purging for 1 hour in our system was ~3 μM.

3.5 Introducing a tryptophan to the dimer interface.

The F355W dimer interface variant showed the same kinetic properties and thermal stability as the wild-type VAP (Table 1). It displayed an increase in fluorometric emission intensity compared to wild-type VAP and a slight red-shift, where λ_{max} was 340.9 ± 0.2 nm (Table 2). The Stern-Volmer constant increased to 3.2 ± 0.2 M^{-1}, indicating that a Trp at position F355 is more exposed on average than the other Trp residues. It was also relatively unquenched in the native state of VAP as judged by its high contribution in the emission spectrum.

3.6 Urea induced denaturation/inactivation for wild-type and F355W.

The urea denaturation and inactivation curves for the wild-type VAP and F355W are shown in Figure 5A. Inactivation was an irreversible step while the unfolding step was partially reversible as monitored by the peak of fluoresence emission (data not shown). The denaturation curve for the wild-type VAP showed the characteristics of a two-state unfolding pathway in the 2 – 4 M urea range with no detectable intermediates. It can also be seen, that the activity fell rapidly with increasing concentration of urea, where half of the activity was lost at 0.3-0.4 M urea. The F355W inactivation curve was identical to the curve for the wild-type VAP. However, the unfolding curve occurring at higher urea concentrations was somewhat different. For the wild-type VAP, unfolding seems to be occurring in the 2 – 4 M range, but for W355 a larger curvature (red-shift) was seen in the unfolding curve starting at around 0.8 M urea. This could be due to solvent exposure of W355 upon dimer dissociation, since the activity had dropped down to less than 15% at 0.8 M urea. This suggested the possibility that an inactive dimeric intermediate was formed before its dissociation took place. Thus, the unfolding scheme is either of the two following cases:

$$\textbf{Case 1:} \quad N_2 \rightarrow I_2 \rightarrow 2I \rightarrow 2U$$

$$\textbf{Case 2:} \quad N_2 \rightarrow I_2 \rightarrow 2U$$

The unfolding curve for the F355W variant could be fitted a four state model (Case 1), where first the inactive dimer is formed $N_2 \rightarrow I_2$ (inactivation is not seen using fluorescence since no dissociation happens). Then, the fluorescence unfolding curve could be fitted with the $I_2 \rightarrow 2I \rightarrow 2D$ model, or $I_2 \rightarrow 2D$, where no folded monomer intermediate accumulates (Case 2). The signal for the possible $I_2 \rightarrow 2I$ conversion (seen by a red-shift) is low and partially merges with the $2I \rightarrow 2D$ conversion, making this observation qualitative at most and making it difficult to distinguish between case 1 or case 2 using F355W fluorescence for detection.

FIGURE 5 here

In an attempt to resolve between case 1 or case 2, we incubated VAP in 8-Anilinonaphthalene-1-sulfonic acid (ANS), which is widely used to detect structural changes resulting in solvent exposure of hydrophobic residues. Surprisingly, VAP showed no increase in fluorescence of ANS over blank measurements in the range 0 – 5 M urea (Figure S2-A) and the signal was not protein concentration dependent (Figure S2-B). Bovine serum albumin (BSA) which is known to readily bind ANS in the native state [38] was used as a control for the experiment and showed the expected increase in ANS fluorescence.

Size exclusion chromatography (SEC) was used to detect the oligomeric state of VAP at 0 M, 1 M, and 2 M urea (Figure 5B). At 0 M urea the enzyme migrates as a 110 kDa protein on the column which fits well to the calculated mass of 112 KDa. At 1 M urea, the dimeric peak is present and starts to split towards a species with lower molecular mass (the monomer). Thus, the observation that dimer dissociation starts around 0.8 M urea using F355W fluorescence (Figure 5A) seems to be correct. In Figure 5A, it can be seen that approximately 10-20% of the enzyme should be unfolded at 2 M urea (if two-state monomer unfolding is assumed). Thus, case 2 ($N_2 \rightarrow I_2 \rightarrow 2I \rightarrow 2U$) seems to be the correct model as two states were seen at 2 M urea, folded monomer and unfolded monomer, where the latter migrates as a larger species than the dimer. However, the molecular mass of the folded monomer in SEC did not fit exactly the calculated mass of 56 kDa but migrates as a 79 kDa species. It is possible that the folded monomers are partially unfolded at some extent at 2 M urea, thus they migrate as a larger protein.

4 Discussion

The aim of this study was to clarify the inactivation and unfolding mechanism of VAP to understand better what factors makes this cold adapted enzyme so susceptible to heat and

urea. The global stability of the enzyme to heat (usually measured by melting temperature) is much greater than the stability of the active-site, but it was not clear if inactivation was due to dissociation of the active dimer or other causes. Here our goal was to use fluorescence to study subtle structural changes upon enzyme inactivation induced by urea. We first characterized the role of each tryptophan in the emission spectrum together with solvent accessibility to define which parts of the enzyme reflected most of the emission spectrum. However, our results showed that none of the native tryptophan residues could serve as a probe for structural changes in the urea induced denaturation experiment. Introducing a tryptophan residue at the dimer interface indicated that an inactive dimer intermediate was formed and this was confirmed by size exclusion chromatography.

4.1 Using tryptophan fluorescence to detect structural changes in VAP

For proteins having multiple Trp residues, it is sometimes feasible to make the Trp fewer by site-directed mutagenesis to decrease the complexity of their fluorescence emission signal. Tyrosine emission is used to a much lesser extent to examine protein folding and dynamics due its higher abundance and lower emission. In order to be able to resolve fluorescence decay spectra, the number of Trp must in most cases be reduced to either one or two, since each Trp is frequently observed having more than one lifetime (e.g. due to rotameric states). For a multi-tryptophan containing protein, the lifetime distribution can be examined as was done with β-glycosidase from the thermophile *S. solfataricus* containing 17 Trp per subunit [39]. In such cases, the relative amplitude of lifetimes of the components is often categorized to a short and long lifetime component by distribution functions. For the fluorescence decay of VAP, it was possible to see a slight decrease in the relative amplitude of the shorter mean-lifetime using Top-hat distribution model (Figure S3) for the removal of the two exposed W274 (in the active site) and W512 (located on StrepTag), indicating that these two residues have shorter lifetimes on average than the rest of the tryptophans.

It would be ideal to reduce the number of Trp residues to either one or two residues and characterize the effect of each on the steady state fluorescence emission of VAP dimers. For *E. coli* cystathionine β-lyase, the complex urea unfolding curve of this homo-tetramer containing six Trp residues was resolved by site-directed mutagenesis. Thus, one Trp residue located at the interface could be used to probe local conformational changes [40]. The urea unfolding curve of native VAP had much less complexity and showed a typical two-state unfolding. Either the dissociation event of dimers was not “felt” by any of the native Trp residues, or no folded monomeric intermediate exist in the unfolding pathway. It is widely accepted that alkaline phosphatases dissociate to inactive monomers. Examples can be seen for ECAP [31] and another cold-active AP from cod [27, 41].

Here we found, using single Trp substitution variants, that two of the conserved Trp residues, W301 and W460, are mostly responsible for the Trp fluorescent emission from VAP. Surprisingly, replacing the tryptophan in the active site (W274F), increased emission compared to the wild-type VAP, indicating that some rearrangement around its Trp residues was taking place. Most likely, another Trp residue was relieved of static quenching. Prior experiments have indicated that W274 plays an indirect role in substrate binding, since W274K [22], W274H [23], W274A (unpublished results) and W274F all caused an approximately two-fold increase in K_M.

It was apparent from the acrylamide quenching studies, that W460 was highly buried in the protein core. Knowing that W460 is a highly buried residue, and produces almost half of the fluorescence emission, it was unexpected to see that the red-shift upon the W460F replacement was not more than approximately 1 nm. However, a high increase in the Stern-Volmer constant, as observed, is either a sign of the loss of highly buried tryptophan emission, or due to a conformational change allowing better access of the quencher.

4.2 Most tryptophan residues in VAP are important for activity and stability.

All the Trp to Phe substitutions in VAP resulted in lower T_m values, an indication of monomer destabilization. Substituting a buried Trp with a Phe residue should leave a hole where the Trp pyrrole ring has been "removed". The lost hydrophobic contacts will likely result in some local alteration of the tertiary structure that may affect distal parts too. The most buried tryptophans, namely W155 (as judged by the crystal structure) and W460, displayed a decreased T_m value by 2-3 °C. Trp to Phe substitutions for solvent exposed Trp should not affect protein stability, at least not when Trp is variably introduced at non-conserved, solvent exposable sites [42, 43]. This is true for the W512F substitution of the highly exposed Trp located on the C-terminal StrepTag. However, a larger decrease in T_m of 4°C was observed for the W274F variant, located at an exposed spot in the active site, than the buried W155F or W460F. The W475F variant had a T_m of 3°C lower than the wild-type, while W301F had a T_m of 6°C lower. These differences can be regarded as very large compared with our previous experience with VAP variants [22, 23]. The W301F mutation clearly affected the folding process in an unknown way resulting in very low expression yields for that variant.

We found that a correlation between solvent exposure of the various Trp in VAP, as estimated from the crystal structure, and the effect on protein stability of Trp-Phe substitutions was not always consequential. A recent example can be found in the literature where the replacement of a highly exposed Trp at a dimer interface with phenylalanine increased stability [44].

All the Trp to Phe substitutions resulted in decreased k_{cat} values, except in case of the solvent exposed W274F and W512F. However, K_M was generally not affected, except for W274F and W460F, where it was increased. It is not clear why k_{cat} is so highly reduced by the replacement of W475F, since W475F is located far from the active site. A loosening of the global fold would be expected going from a larger residue, having more contacts, to a smaller residue having fewer contacts. However, it is likely that the packing of the hydrophobic core is affected by the Trp $\rightarrow$ Phe substitutions since the sum of difference spectra was not identical to the wild-type VAP and was blue-shifted. This could reach afar through networks shaping distribution of intra- and intermolecular interactions [45].

K_M was increased for the active-site W274F variant (and other W274 variants) but k_{cat} was unaffected. W274, which is equivalent to K328 í ECAP, has no direct contacts with the substrate but coordinates a water molecule which is a part of tight water molecule network around the M3 site. The coordinated waters in the active site might help accommodate the hydrated substrate when it binds.

The W460F replacement caused a lower affinity for the substrate despite the fact that this residue is located 15 Å away from the active site. Furthermore, the W460Y VAP variant had only a slight effect on k_{cat} and K_M, showing that either Trp or Tyr is preferred at this site as the W460I variant was completely inactive. The unexpected increase in K_M for W460F could be rationalized by the consideration that a phenylalanine in that positions is unable to have favorable polar-polar interactions with Asn279. Asn279 is located on a helix-turn-helix loop in the active site, close to His277 and Asp273 that are both M1 coordinates for Zn (Figure 6). Furthermore, His465, another M1 coordinate, is located on a short ß-strand upstream of the loop where W460 is located. Thus, increased mobility of this short loop (magenta in Figure 6) could allow for movement of zinc ion coordinates and disfavor substrate binding by the zinc ion.

FIGURE 6 here

For APs in general, an aromatic residue is conserved at the corresponding site occupied by Trp460. For ECAP and human placenta alkaline phosphatase (PLAP), there is a Tyr residue at this site. For cold-adapted APs, the residue corresponding to W460 is a Trp residue in *Shewenella* AP [46-48] and *Cobetia marina* AP [49], while it is a Tyr residue in APs from Antarctic shrimp [8] and the Antarctic bacterium TAB5 AP [14, 50]. Notably, all of the cold adapted variants mentioned here have an Asn residue at same position as Asn279 in VAP.

4.3. Phosphorescence of VAP

All proteins that contain Trp are phosphorescent if the viscosity and/or temperature is lowered to 77K [51]. The radiation-less decay of the excited triplet state in solvents is very

dependent on solvent viscosity. Thus, a very low triplet state lifetime at room temperature is observed for solvent exposed Trp, while deeply buried Trp can have a lifetime of several orders of magnitude higher (reviewed in [52]). In a survey where protein phosphorescence at room temperature was tested for 39 proteins, the phosphorescence lifetimes in the range 0.5 ms to 2 s were observed for three-fourths of the proteins tested [53]. Only nine proteins had no detected phosphorescence, while seven proteins had lifetimes greater than 100 ms.

Here, VAP was shown to be phosphorescent at room temperature, having two lifetimes, where the longer lifetime was 140 ms and due to W460 phosphorescence. It was not possible to resolve which Trp residue was responsible for the shorter lifetime, since the margins of repeated measurements were around 30%. We believe that this can be explained by less than optimal deoxygenation of the samples, letting argon gas bubble slowly through a 500 µl quartz flow cell. To test the efficiency of deoxygenation, a protein sample with a known bimolecular quenching constant was measured using the same purging conditions. Alkaline phosphatase from *E. coli* (ECAP) has a well-known bimolecular quenching constant where Trp 109 in ECAP has the highest reported phosphorescence lifetimes for a protein at room temperature. Measuring ECAP under an identical condition to that used for VAP showed that ECAP had one phosphorescence lifetime of 230 ms. The reported lifetime without any oxygen is close to 2 s at room temperature in the literature [30]. We are currently optimizing a new deoxygenation method, since having a phosphorescent protein at room temperature opens up many possibilities to study dynamics and conformational changes on the millisecond to second timescale which is the timescale of protein collective domain motions. As an example, protein phosphorescence has been useful in studying affinities for inorganic phosphate in ECAP, where the phosphorescent Trp109 is located near the active site [29]. The structural role of metal ion binding in ECAP [7], slow structure rearrangement upon reactivation of ECAP [54] and hydrogen exchange in the core of ECAP [55] were also studied by measuring phosphorescence. The phosphorescence of several proteins was used to elegantly show that acrylamide was capable of long range quenching without the requirement of direct penetration, as well as how conformational fluctuations can be probed by quenchers of different sizes [56].

Returning to VAP, we would like to see if the phosphorescence of W460 could serve as a more sensitive probe than fluorescence probe for reporting on the dissociation of dimers, since its backbone position is facing the subunit interface. The two phosphorescence lifetimes reported here for VAP, could be used to study VAP subunit heterogeneity in the millisecond to second timescale with reference to the heterogeneous activity of subunits [57-61] and asymmetric flexibility [45] reported for other APs.

4.4 Detection of a dimer intermediate and mechanism for inactivation and unfolding.

We have shown here, that the effect on kinetics and thermal stability was too great for single Trp substitutions to make it possible to leave either one or two Trp intact and expect the variant to reflect the state of the native VAP structure.

Introducing a new Trp residue by site directed mutagenesis at the subunit interface (position F355) was shown to have no effect on the steady-state kinetic constants or stability of the enzyme. Furthermore, an emission red-shift in the 0.8-1.8 M urea range was observed as a small curvature in the urea denaturation curve for F355W, an indication of an increased polarity around the F355W residue. For F355W (as well as the wild-type VAP), almost all activity of the enzyme was lost at 1 M urea concentration. Thus, if the red-shift seen at around 1-2 M urea was the dimer dissociation event, the inactivation induced by urea was a consequence of formation of an inactive dimer or a dimeric state with trace activity present. We have previously reported on an increase in the mobility of a spin probe in the 1-2 M urea range when located on the only native Cys67 residue close to the active site [23]. The wild-type VAP did not show as distinct a red-shift curvature at this range before unfolding took place. SEC data indicated that the enzyme was still in the dimeric form at 1 M urea and completely monomeric at 2 M urea. Thus, the correct model for inactivation and unfolding involves an inactive dimeric intermediate and a folded monomeric state before the monomers unfold: $N_2 \rightarrow I_2 \rightarrow 2I \rightarrow 2D$. This is the first example of an inactive alkaline phosphatase dimeric state induced by a denaturant. In the literature, there are not many examples of inactive dimer intermediate states induced by denaturants for other enzymes. Some examples include guanidine hydrochloride mediated denaturation of *E. coli* alanyl-tRNA synthetase [62] and organophosphorus hydrolase from *Pseudomonas diminuta* [63]. Commonly, the active-site is usually more stable to denaturants than the dimer interface, and cold adapted enzymes are probably more prone to form inactive dimer intermediates than mesophilic ones.

The inactivation event in VAP might be facilitated by a dissociation of Mg^{2+} from the active site or rearrangement of key residues involved in substrate activation such as Arg129 (homologous to Arg166 in *E. coli*). Arg129 is crucial for substrate binding [64], activation and possibly for modulation of negative cooperativity in half-of-sites reactivity [65].

VAP has one of the highest catalytic activities at lower temperatures found in APs, which is likely promoted by more loop mobility around the active site. Therefore, it does not come by surprise that the active-site might be more prone to adapt kinetically unfavorable rearrangements of key residue compared with more heat-tolerant APs, especially the ones that coordinate the active site metal ions. Thus, low concentration of a chaotropic denaturant might facilitate the transition to this inactive and kinetically trapped state. More experiments need to be conducted to evaluate the nature of this inactive dimeric state, such as conducting crystallographic experiments at low urea concentrations. We strongly believe that magnesium

might be absent in the inactive dimeric structure. We are currently optimizing magnesium dissociation assays for VAP. However, it is very challenging to measure the dissociation of magnesium from the active site where a bias for magnesium dissociation exists, since leakage of magnesium during sample preparation and handling of the enzyme is common (e.g. dialysis or desalting).

Conclusion

In this study, we have characterized all the tryptophan residues in VAP with respect to fluorescence, activity and stability. One residue close to the active site, excluded from the solvent (W460), is highly phosphorescent and plays a distant role in modulating substrate binding. By studying the inactivation and unfolding mechanism using urea as a denaturant, the enzyme was found to form an inactive dimeric intermediate state that is structurally similar to the active state. This is the first time to our knowledge that alkaline phosphatase is shown to have an inactive dimeric state not promoted by mutagenesis or chemical inhibition.

Acknowledgements

Financial support from the Icelandic Research Fund (project 141619-051) and the Science Institute of the University of Iceland is gratefully acknowledged.

References

[1] A. Shurki, E. Derat, A. Barrozo, S.C. Kamerlin, How valence bond theory can help you understand your (bio)chemical reaction, Chem Soc Rev, 44 (2015) 1037-1052.
[2] F. Duarte, J. Aqvist, N.H. Williams, S.C. Kamerlin, Resolving apparent conflicts between theoretical and experimental models of phosphate monoester hydrolysis, J Am Chem Soc, 137 (2015) 1081-1093.
[3] F. Sunden, A. Peck, J. Salzman, S. Ressl, D. Herschlag, Extensive site-directed mutagenesis reveals interconnected functional units in the alkaline phosphatase active site, Elife, 4 (2015).
[4] M. Gottesman, R.T. Simpson, B.L. Vallee, Kinetic properties of cobalt alkaline phosphatase, Biochemistry, 8 (1969) 3776-3783.
[5] J. Wang, K.A. Stieglitz, E.R. Kantrowitz, Metal specificity is correlated with two crucial active site residues in *Escherichia coli* alkaline phosphatase, Biochemistry, 44 (2005) 8378-8386.
[6] N. Gong, C. Chen, L. Xie, H. Chen, X. Lin, R. Zhang, Characterization of a thermostable alkaline phosphatase from a novel species *Thermus yunnanensi*s sp. nov. and investigation of its cobalt activation at high temperature, Biochim Biophys Acta, 1750 (2005) 103-111.
[7] P. Cioni, L. Piras, G.B. Strambini, Tryptophan phosphorescence as a monitor of the structural role of metal ions in alkaline phosphatase, Eur J Biochem, 185 (1989) 573-579.
[8] M. de Backer, S. McSweeney, H.B. Rasmussen, B.W. Riise, P. Lindley, E. Hough, The 1.9 Ångstrom crystal structure of heat-labile shrimp alkaline phosphatase, J Mol Biol, 318 (2002) 1265-1274.

[9] C.L. Wojciechowski, E.R. Kantrowitz, Altering of the metal specificity of *Escherichia coli* alkaline phosphatase, J Biol Chem, 277 (2002) 50476-50481.
[10] L. Ma, T.T. Tibbitts, E.R. Kantrowitz, *Escherichia coli* alkaline phosphatase: X-ray structural studies of a mutant enzyme (His-412-->Asn) at one of the catalytically important zinc binding sites, Protein Sci, 4 (1995) 1498-1506.
[11] M. Bortolato, F. Besson, B. Roux, Role of metal ions on the secondary and quaternary structure of alkaline phosphatase from bovine intestinal mucosa, Proteins-Struct Funct Genet, 37 (1999) 310-318.
[12] G. Cathala, C. Brunel, D. Chappelettordo, M. Lazdunski, Bovine kidney alkaline-phosphatase - catalytic properties, subunit interactions in catalytic process, and mechanism of Mg^{2+} Stimulation, J Biol Chem, 250 (1975) 6046-6053.
[13] B. Stec, K.M. Holtz, E.R. Kantrowitz, A revised mechanism for the alkaline phosphatase reaction involving three metal ions, J Mol Biol, 299 (2000) 1303-1311.
[14] E. Wang, D. Koutsioulis, H.K. Leiros, O.A. Andersen, V. Bouriotis, E. Hough, P. Heikinheimo, Crystal structure of alkaline phosphatase from the Antarctic bacterium TAB5, J Mol Biol, 366 (2007) 1318-1331.
[15] A. Garen, C. Levinthal, A fine-structure genetic and chemical study of the enzyme alkaline phosphatase of E. coli. I. Purification and characterization of alkaline phosphatase, Biochim Biophys Acta, 38 (1960) 470-483.
[16] M.H. Malamy, B.L. Horecker, Purification and crystallization of the alkaline phosphatase of *Escherichia coli*, Biochemistry, 3 (1964) 1893-1897.
[17] X.J. Tian, X.H. Song, S.L. Yan, Y.X. Zhang, H.M. Zhou, Study of refolding of calf intestinal alkaline phosphatase, J Prot Chem, 22 (2003) 417-422.
[18] R.B. McComb, G.N. Bowers, S. Posen, Alkaline phosphatase, Plenum Press, 1979, pp. 198-199, 330-332.
[19] J.G. Zalatan, T.D. Fenn, D. Herschlag, Comparative enzymology in the alkaline phosphatase superfamily to determine the catalytic role of an active-site metal ion, J Mol Biol, 384 (2008) 1174-1189.
[20] J. Hauksson, O. Andresson, B. Asgeirsson, Heat-labile bacterial alkaline phosphatase from a marine *Vibrio* sp, Enzym Microbiol Technol, 27 (2000) 66-73.
[21] R. Helland, R.L. Larsen, B. Asgeirsson, The 1.4 Ångstrom crystal structure of the large and cold-active *Vibrio* sp. alkaline phosphatase, Biochim Biophys Acta-Proteins and Proteomics, 1794 (2009) 297-308.
[22] K. Gudjonsdottir, B. Asgeirsson, Effects of replacing active site residues in a cold-active alkaline phosphatase with those found in its mesophilic counterpart from *Escherichia coli*, FEBS J, 275 (2008) 117-127.
[23] P.O. Heidarsson, S.T. Sigurdsson, B. Asgeirsson, Structural features and dynamics of a cold-adapted alkaline phosphatase studied by EPR spectroscopy, FEBS J, 276 (2009) 2725-2735.
[24] I.S. Krull, H.H. Stuting, S.C. Krzysko, Conformational studies of bovine alkaline phosphatase in hydrophobic interaction and size-exclusion chromatography with linear diode array and low-angle laser light scattering detection, J Chromatogr, 442 (1988) 29-52.
[25] M.L. Applebury, J.E. Coleman, *Escherichia coli* alkaline phosphatase. Metal binding, protein conformation, and quaternary structure, J Biol Chem, 244 (1969) 308-318.
[26] M.J. Schlesinger, K. Barrett, The reversible dissociation of the alkaline phosphatase of *Escherichia coli*. I. Formation and reactivation of subunits, J Biol Chem, 240 (1965) 4284-4292.
[27] B. Asgeirsson, K. Gudjonsdottir, Reversible inactivation of alkaline phosphatase from Atlantic cod (*Gadus morhua*) in urea, Biochim Biophys Acta-Proteins and Proteomics, 1764 (2006) 190-198.
[28] R.L. Olsen, K. Overbo, B. Myrnes, Alkaline-phosphatase from the hepatopancreas of shrimp (*Pandalus Borealis*) - a dimeric enzyme with catalytically active subunits, Comp Biochem Phys B, 99 (1991) 755-761.

[29] L. Sun, E.R. Kantrowitz, W.C. Galley, Room temperature phosphorescence study of phosphate binding in *Escherichia coli* alkaline phosphatase, Eur J Biochem, 245 (1997) 32-39.
[30] M. Gonnelli, G.B. Strambini, Phosphorescence lifetime of tryptophan in proteins, Biochemistry, 34 (1995) 13847-13857.
[31] R.R. Boulanger, Jr., E.R. Kantrowitz, Characterization of a monomeric *Escherichia coli* alkaline phosphatase formed upon a single amino acid substitution, J Biol Chem, 278 (2003) 23497-23501.
[32] M.R. Eftink, C.A. Ghiron, Exposure of tryptophanyl residues and protein dynamics, Biochemistry, 16 (1977) 5546-5551.
[33] G.B. Strambini, M. Gonnelli, Acrylonitrile quenching of trp phosphorescence in proteins: a probe of the internal flexibility of the globular fold, Biophys J 99 (2010) 944-952.
[34] G.B. Strambini, M. Gonnelli, Protein phosphorescence quenching: distinction between quencher penetration and external quenching mechanisms, J Phys Chem B, 114 (2010) 9691-9697.
[35] M. Niklasson, C. Andresen, S. Helander, M.G. Roth, A. Zimdahl Kahlin, M. Lindqvist Appell, L.G. Martensson, P. Lundstrom, Robust and convenient analysis of protein thermal and chemical stability, Protein Sci (2015) 2055-2062.
[36] C.N. Pace, F. Vajdos, L. Fee, G. Grimsley, T. Gray, How to measure and predict the molar absorption coefficient of a protein, Prot Sci, 4 (1995) 2411-2424.
[37] P. Cioni, G.B. Strambini, Pressure/temperature effects on protein flexibilty from acrylamide quenching of protein phosphorescence, J Mol Biol, 291 (1999) 955-964.
[38] D.M. Togashi, A.G. Ryder, A fluorescence analysis of ANS bound to bovine serum albumin: binding properties revisited by using energy transfer, J Fluor, 18 (2008) 519-526.
[39] E. Bismuto, G. Irace, S. D'Auria, M. Rossi, R. Nucci, Multitryptophan-fluorescence-emission decay of beta-glycosidase from the extremely thermophilic archaeon *Sulfolobus solfataricus*, Eur J Biochem, 244 (1997) 53-58.
[40] A.F. Jaworski, S.M. Aitken, Exploration of the six tryptophan residues of *Escherichia coli* cystathionine beta-lyase as probes of enzyme conformational change, Arch Biochem Biophys, 538 (2013) 138-144.
[41] B. Asgeirsson, J. Hauksson, G. Gunnarsson, Dissociation and unfolding of cold-active alkaline phosphatase from Atlantic cod in the presence of guanidinium chloride, Eur J Biochem, 267 (2000) 6403-6412.
[42] H. Gu, N. Doshi, D.E. Kim, K.T. Simons, J.V. Santiago, S. Nauli, D. Baker, Robustness of protein folding kinetics to surface hydrophobic substitutions, Protein Sci, 8 (1999) 2734-2741.
[43] A. Vallee-Belisle, S.W. Michnick, Visualizing transient protein-folding intermediates by tryptophan-scanning mutagenesis, Nat Struct Mol Biol, 19 (2012) 731-+.
[44] Z. Markovic-Housley, B. Stolz, R. Lanz, B. Erni, Effects of tryptophan to phenylalanine substitutions on the structure, stability, and enzyme activity of the IIAB(Man) subunit of the mannose transporter of *Escherichia coli*, Protein Sci, 8 (1999) 1530-1535.
[45] B. Asgeirsson, G. Renzetti, G. Invernizzi, E. Papaleo, Asymmetric flexibility of a homodimeric enzyme as shown by molecular dynamics computations. A case study of the cold-active *Vibrio* alkaline phosphatase, FEBS Journal, 280 (2013) 157.
[46] H. Tsuruta, B. Mikami, T. Higashi, Y. Aizono, Crystal structure of cold-active alkaline phosphatase from the psychrophile *Shewanella sp*, Biosci Biotechnol Biochem, 74 (2010) 69-74.
[47] T. Murakawa, H. Yamagata, H. Tsuruta, Y. Aizono, Cloning of cold-active alkaline phosphatase gene of a psychrophile, *Shewanella sp*., and expression of the recombinant enzyme, Biosci Biotechnol Biochem, 66 (2002) 754-761.
[48] Y. Suzuki, Y. Mizutani, T. Tsuji, N. Ohtani, K. Takano, M. Haruki, M. Morikawa, S. Kanaya, Gene cloning, overproduction, and characterization of thermolabile alkaline phosphatase from a psychrotrophic bacterium, Biosci Biotechnol Biochem, 69 (2005) 364-373.

[49] V. Golotin, L. Balabanova, G. Likhatskaya, V. Rasskazov, Recombinant production and characterization of a highly active alkaline phosphatase from marine bacterium *Cobetia marina*, Mar Biotechnol (NY), 17 (2015) 130-143.
[50] M. Rina, C. Pozidis, K. Mavromatis, M. Tzanodaskalaki, M. Kokkinidis, V. Bouriotis, Alkaline phosphatase from the Antarctic strain TAB5. Properties and psychrophilic adaptations, Eur J Biochem, 267 (2000) 1230-1238.
[51] M.L. Saviotti, W.C. Galley, Room temperature phosphorescence and the dynamic aspects of protein structure, Proc Natl Acad Sci U S A, 71 (1974) 4154-4158.
[52] P. Cioni, G.B. Strambini, Tryptophan phosphorescence and pressure effects on protein structure, Biochim Biophys Acta, 1595 (2002) 116-130.
[53] J.M. Vanderkooi, D.B. Calhoun, S.W. Englander, On the prevalence of room-temperature protein phosphorescence, Science, 236 (1987) 568-569.
[54] V. Subramaniam, N.C. Bergenhem, A. Gafni, D.G. Steel, Phosphorescence reveals a continued slow annealing of the protein core following reactivation of *Escherichia coli* alkaline phosphatase, Biochemistry, 34 (1995) 1133-1136.
[55] C.J. Fischer, J.A. Schauerte, K.C. Wisser, A. Gafni, D.G. Steel, Hydrogen exchange at the core of *Escherichia coli* alkaline phosphatase studied by room-temperature tryptophan phosphorescence, Biochemistry, 39 (2000) 1455-1461.
[56] G.B. Strambini, M. Gonnelli, Influence of denaturants on native-state structural fluctuations in azurin probed by molecular size-dependent quenching of Trp phosphorescence, J Phys Chem B, 115 (2011) 13755-13764.
[57] D. Chappelet-Tordo, M. Fosset, M. Iwatsubo, C. Gache, M. Lazdunski, Intestinal alkaline phosphatase. Catalytic properties and half of the sites reactivity, Biochemistry, 13 (1974) 1788-1795.
[58] D. Chappelet-Tordo, M. Iwatsubo, M. Lazdunski, Negative cooperativity and half of the sites reactivity. Alkaline phosphatases of *Escherichia coli* with Zn^{2+}, Co^{2+}, Cd^{2+}, Mn^{2+}, and Cu^{2+} in the active sites, Biochemistry, 13 (1974) 3754-3762.
[59] S. Orhanovic, M. Pavela-Vrancic, Dimer asymmetry and the catalytic cycle of alkaline phosphatase from *Escherichia coli*, Eur J Biochem, 270 (2003) 4356-4364.
[60] P. Gettins, J.E. Coleman, ^{31}P nuclear magnetic resonance of phosphoenzyme intermediates of alkaline phosphatase, J Biol Chem, 258 (1983) 408-416.
[61] M.F. Hoylaerts, T. Manes, J.L. Millan, Mammalian alkaline phosphatases are allosteric enzymes, J Biol Chem, 272 (1997) 22781-22787.
[62] B. Banerjee, R. Banerjee, Guanidine hydrochloride mediated denaturation of *E. coli* Alanyl-tRNA synthetase: identification of an inactive dimeric intermediate, Protein J, 33 (2014) 119-127.
[63] J.K. Grimsley, J.M. Scholtz, C.N. Pace, J.R. Wild, Organophosphorus hydrolase is a remarkably stable enzyme that unfolds through a homodimeric intermediate, Biochemistry, 36 (1997) 14366-14374.
[64] A. Chaidaroglou, D.J. Brezinski, S.A. Middleton, E.R. Kantrowitz, Function of arginine-166 in the active site of *Escherichia coli* alkaline phosphatase, Biochemistry, 27 (1988) 8338-8343.
[65] N.M. Rao, R. Nagaraj, Anomalous stimulation of *Escherichia coli* alkaline phosphatase activity in guanidinium chloride. Modulation of the rate-limiting step and negative cooperativity, J Biol Chem, 266 (1991) 5018-5024.

Tables

Table 1: Kinetic measurements and temperature unfolding. For kinetic measurements the rate of hydrolysis of p-NPP in 0.1 M CAPS, 500 mM NaCl, 1 mM $MgCl_2$, pH 9.8 was measured at 10°C. Temperature unfolding (T_m) was monitored by CD spectroscopy in 25 mM MOPS, 1 mM $MgSO_4$, pH 8.0 (20°C) by measuring a melting curve at 222 nm in the range 15-85 °C. The average data with standard deviations were obtained from several independent experiments (n = 3-5).

Enzyme variant	k_{cat} (s^{-1})	K_m (µM)	k_{cat}/K_m ($s^{-1}mM^{-1}$)	T_m (°C)
Wild-type	302 ± 20	194 ± 30	1560 ± 260	51.0 ± 0.6
W155F	125 ± 2	218 ± 8	573 ± 23	49.8 ± 2.2
W274F	300 ± 4	462 ± 25	650 ± 36	47.1 ± 0.7
W301F	137 ± 8	239 ± 23	573 ± 64	44.6 ± 1.7
W460F	65 ± 4	354 ± 56	184 ± 31	48.7 ± 1.3
W475F	44 ± 2	194 ± 22	230 ± 28	48.1 ± 0.1
W512F	313 ± 36	212 ± 29	1480 ± 260	51.0 ± 0.3
F355W	255 ± 56	218 ± 20	1170 ± 280	52.0 ± 0.9
W460Y	275 ± 41	252 ± 46	869 ± 240	N/A

Table 2: Fluorescence emission maxima and acrylamide quenching data for VAP variants. All samples were prepared in 20 mM MOPS, 1 mM $MgSO_4$, pH 8.0 (corrected for 10°C) to a final enzyme concentration of 0.02 mg/mL. The emission spectra were recorded at 10°C for 310-400 nm using 295 nm as excitation wavelength. Stern-Volmer constants (K_{sv}) were derived as the slope of F_0/F plotted against [acrylamide] quencher. The data represent the average and standard deviation from 2-4 independent experiments.

Enzyme variant	λ_{max} (nm)	K_{sv} (M^{-1})
Wild-type	340.1 ± 0.1	2.4 ± 0.3
W155F	341.1 ± 0.1	2.6 ± 0.1
W274F	339.3 ± 0.2	2.4 ± 0.1
W301F	341.0 ± 0.1	2.3 ± 0.1
W460F	341.4 ± 0.8	7.9 ± 0.2
W475F	342.0 ± 0.1	2.9 ± 0.1
W512F	339.5 ± 0.3	2.8 ± 0.2
F355W	340.9 ± 0.2	3.2 ± 0.2

Figures:

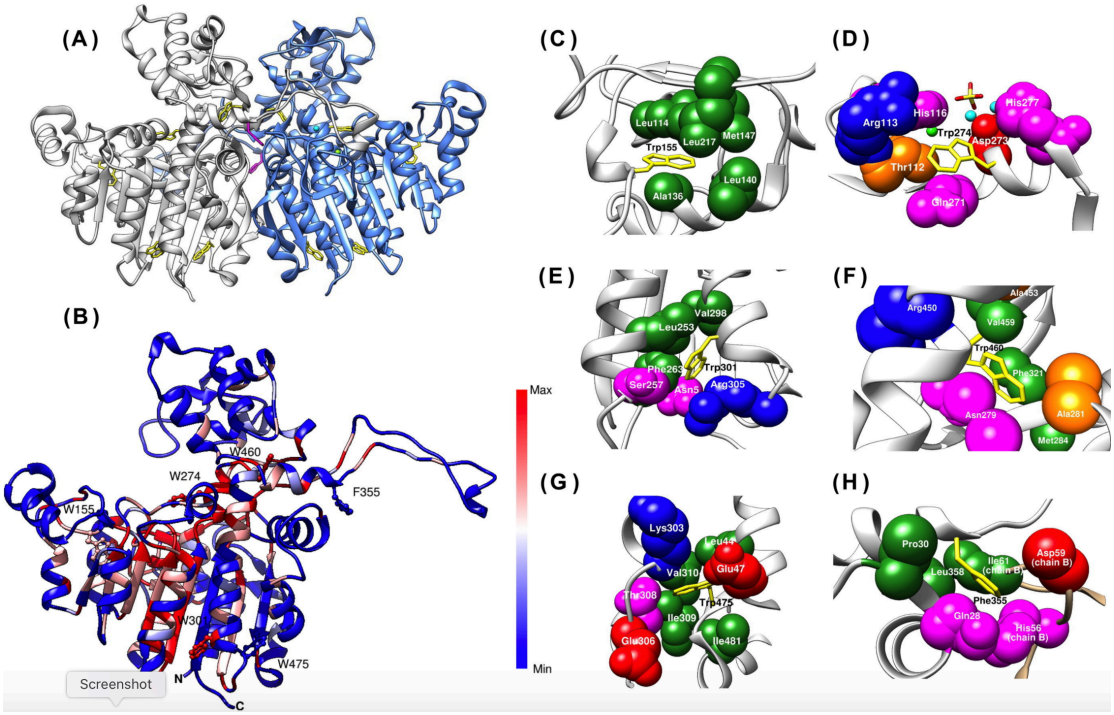

Figure 1. VAP crystal structure (PDB: 3E2D). (A) VAP dimeric structure. Tryptophan residues are colored in yellow, residue F355 in magenta, and Zn and Mg ions in cyan and green, respectively. **(B)** Conservation of residues in the VAP monomer. Conserved sites are shown in red and non-conserved in blue. The five native tryptophans and F355 are shown as balls and sticks. Conservation calculations were done using ConSurf server (UNIREF90 and MAFFT) and the structure rendered in Chimera. **(**C-H) The environment within 5 Å around the chosen native tryptophan residues (C-G, and added Phe355 (H). Tryptophan residues and Phe355 are shown in yellow sticks and neighboring residues as spheres. Hydrophobic residues are shown in green, small non-polar residues in orange, polar residues in magenta, negatively charged residues in red and positively charged residues in blue. Zn and Mg ions are shown in teal and green respectively and sulphate ion as sticks in yellow and red (D).

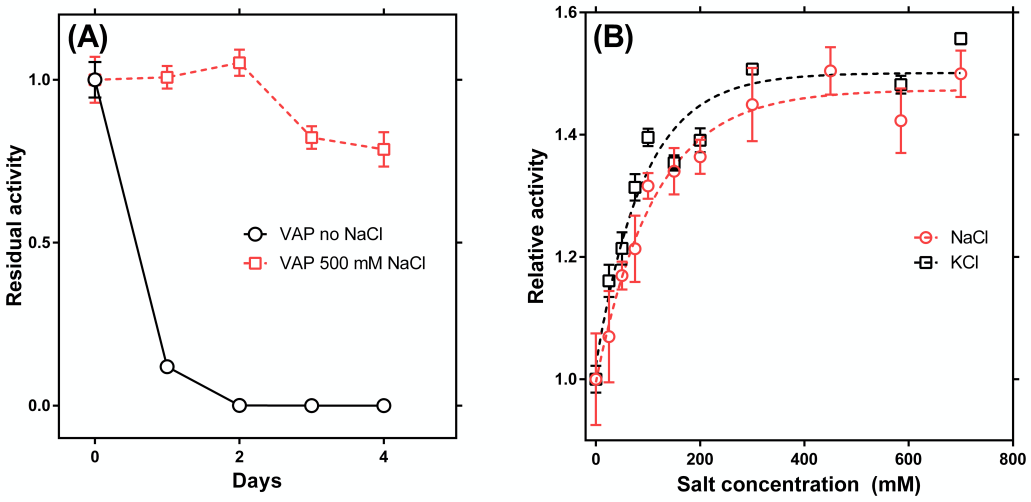

Figure 2: Effect of NaCl on VAP activity and stability. (A) Effect of NaCl on VAP storage at room temperature. Samples were incubated in 25 mM Mops, pH 8.0 and activity measured under trans-phosphorylation of 2.0 mM p-nitrophenyl phosphate (p-NPP) at 25°C in 1.0 M diethanolamine with 1.0 mM $MgCl_2$ at pH 9.8. **(B)** Effect of NaCl and KCl on catalytic turnover. Activity was measured under hydrolysing conditions with 5 mM PNPP, 100 mM Caps, 1 mM $MgCl_2$ with NaCl or KCl ranging from 0-700 mM at pH 9.8 and 10 °C.

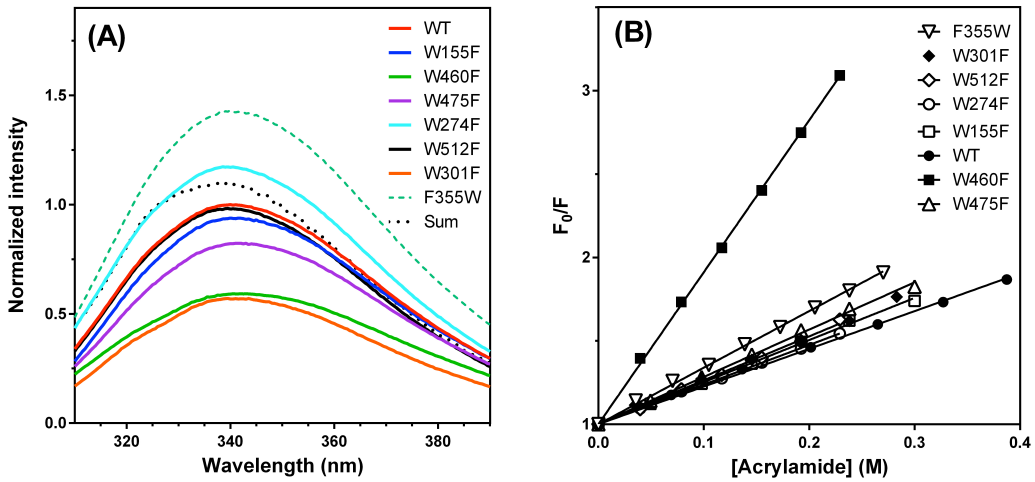

Figure 3. Emission spectra of single tryptophan variants of VAP and acrylamide quenching. (A) Emission spectra were recorded at 10°C in the range 310-390 nm using excitation at 295 nm (5 nm slit-width for both emission and excitation). Blank was measured under the same conditions and subtracted from the spectra. Measurements came from several independent experiments (n = 2-4). The sum spectrum shown is the total of the added difference spectra of Trp → Phe mutants compared to the wild-type VAP spectrum, but excluding the W274F spectrum (black dotted line). Emission intensity was normalized to the wild-type maximum emission intensity **(B)** Stern-Volmer plots. Emission intensity at 340 nm was measured under the same conditions as in (A) after addition of aliquots of acrylamide giving F_0/F, where F_0 is the emission without acrylamide and F the emission after each added aliquot. The Stern-Volmer constant was derived by linear regression in Graphpad Prism.

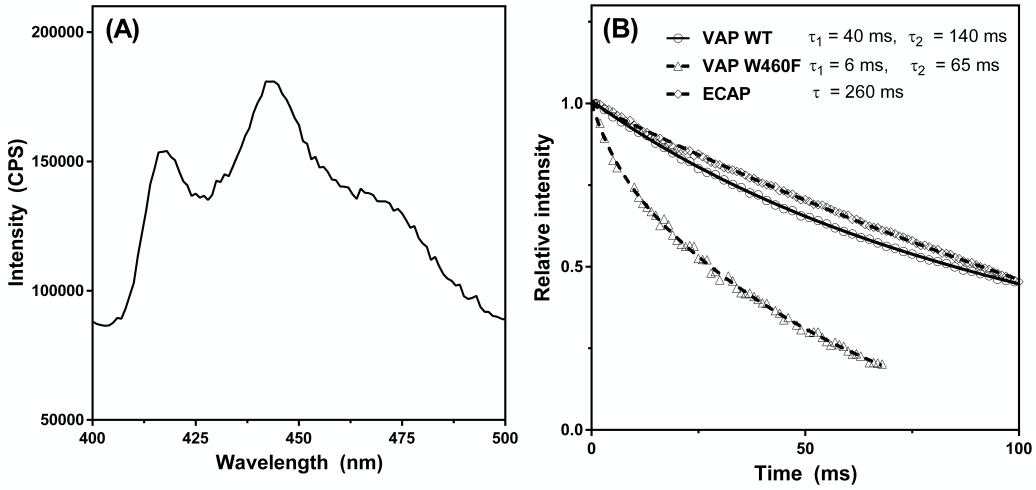

Figure 4. VAP phosphorescence. (A) Phosphorescence emission spectrum of VAP. **(B)** Phosphorescence decay for VAP wild-type, VAP-W460F or ECAP. Data for VAP wild-type and VAP-W460F were fitted to a two exponential decay model, whereas the ECAP data was fitted to a single exponential model using Graphpad Prism.

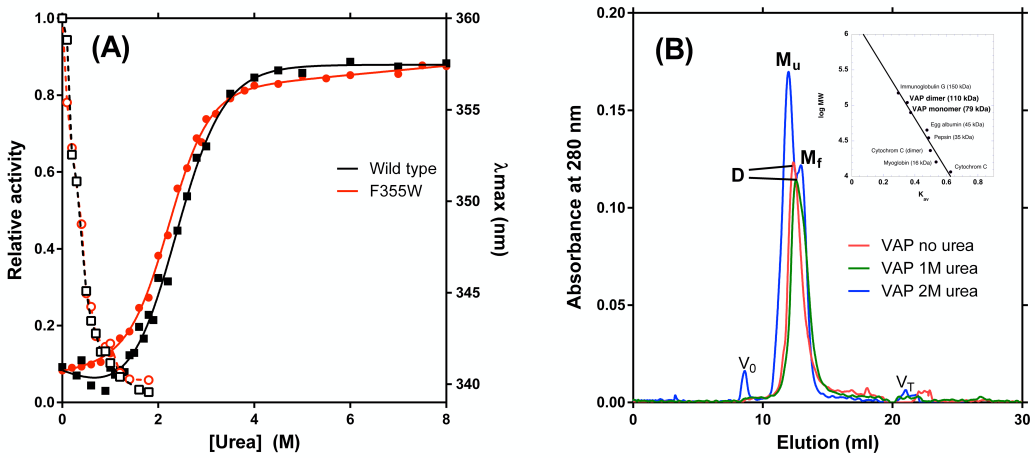

Figure 5. Urea denaturation of VAP. (A) Urea induced fluorescence red-shift and inactivation**.** Samples were incubated in 0 – 8 M urea for 4 h at 10°C before measurements. Inactivation curves for the wild-type VAP are plotted in black with closed and open circles for inactivation and denaturation, respectively. Inactivation curves for F355W are plotted in red with closed and open squares for inactivation and denaturation, respectively. The unfolding curves were fitted to a two-state model for wild-type VAP (N → U) and a three-state model for the F355W variant (I_2 → 2I → 2U). **(B)** Size exclusion chromatography. VAP samples of approximately 1.5 mg/ml were pretreated with 0, 1 or 2 M urea for 4 h at 10 °C in 25 mM Mops, 1 mM $MgSO_4$, pH 8.0 before loading on a Superose 12 column (GE Healthcare) pre-equilibrated in the same denaturant buffer. Protein standard curve is shown as inset. V_t = 20.67 ml and V_o = 8.33 ml. R_f dimer = 12.67 ± 0.39 (n=3) ml ; R_f monomer = 12.97 ±0.25 ml; R_f unfolded monomer = 10.20 ml. V_t, V_0, D, M_f and M_u denote the total volume, void volume, native dimer, folded monomer and unfolded monomer, respectively.

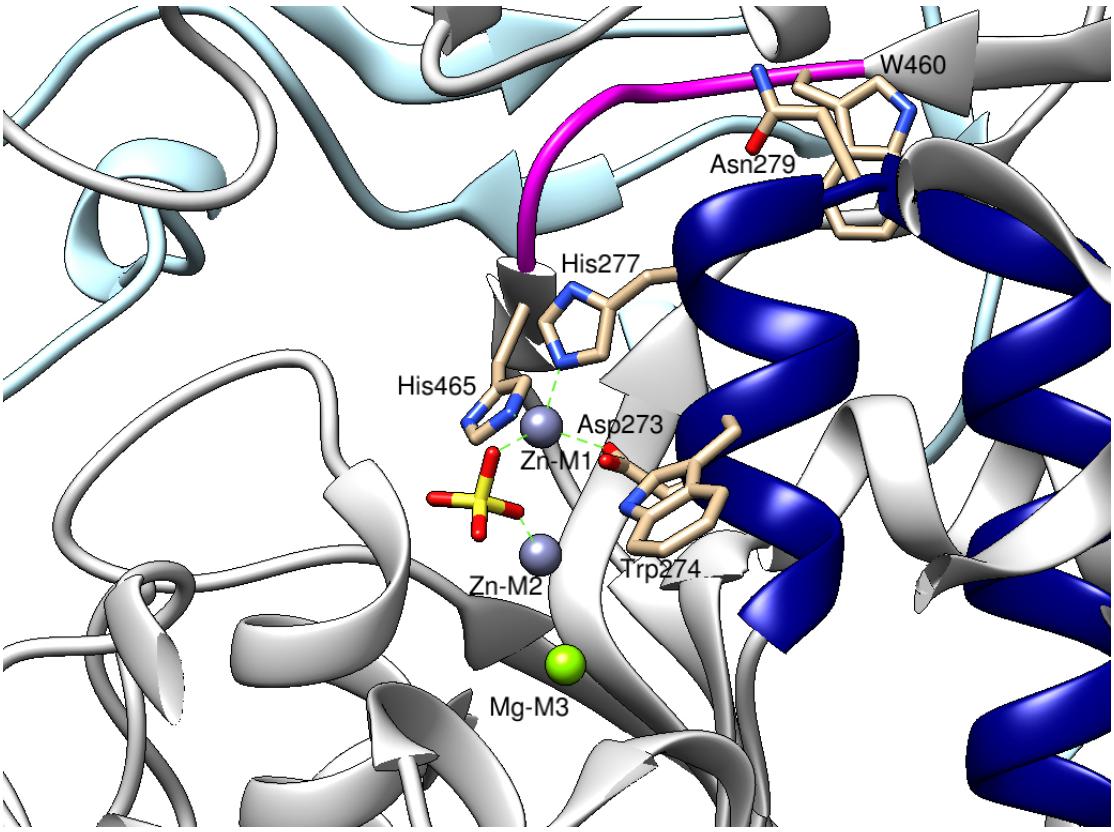

Figure 6. Distal linkage of Trp460 to the active-site. The short loop where Trp460 is located is shown in magenta and the helix-turn-helix where Asn279 and zinc coordinates are located is shown in navy blue. A sulphate ion is shown bound to the active site pocket. It should be noted that not all substrate and metal-ion ligands are shown here for simplicity.

Graphic abstract: